Soft Robotic Burrowing Device with Tip-Extension and Granular Fluidization

Nicholas D. Naclerio[1,*], Christian M. Hubicki[2], Yasemin Ozkan Aydin[2], Daniel I. Goldman[2], and Elliot W. Hawkes[1]

***Abstract*— Mobile robots of all shapes and sizes move through the air, water, and over ground. However, few robots can move through the ground. Not only are the forces resisting movement much greater than in air or water, but the interaction forces are more complicated. Here we propose a soft robotic device that burrows through dry sand while requiring an order of magnitude less force than a similarly sized intruding body. The device leverages the principles of both tip-extension and granular fluidization. Like roots, the device extends from its tip; the principle of tip-extension eliminates skin drag on the sides of the body, because the body is stationary with respect to the medium. We implement this with an everting, pressure-driven thin film body. The second principle, granular fluidization, enables a granular medium to adopt a dynamic fluid-like state when pressurized fluid is passed through it, reducing the forces acting on an object moving through it. We realize granular fluidization with a flow of air through the core of the body that mixes with the medium at the tip. The proposed device could lead to applications such as search and rescue in mudslides or shallow subterranean exploration. Further, because it creates a physical conduit with its body, electrical lines, fluids, or even tools could be passed through this channel.**

I. INTRODUCTION

Subterranean locomotion is a challenging endeavor, due in large part to the substantial forces resisting movement [1]. Most work on moving below ground has been in the field of conventional drilling, where methods include auger drilling, hydraulic-rotary drilling, and tunnel boring machines [2,3]. These methods are effective at creating holes and tunnels through soil and rock, but are not ideal for small subterranean robots due to the power and heavy equipment required. In coastal areas, water jetting is often used to drive piles into soft sand and clay. This method uses a high pressure water jet to fluidize the sand beneath a heavy piling, allowing it to sink under its own weight [4].

Burrowing animals [5,6] and plant roots [7] have inspired several recent attempts to create robots capable of subterranean locomotion. One set of studies replicated the mechanism used by burrowing bivalve clams to burrow into ocean sediment. This work imitates the behavior of clams which use the motion of their shell to fluidize the layer of wet sand surrounding them [8]–[10]. Studies inspired by the apical growth of plant roots used either an everting skin [11] or a filament extruder to burrow with reduced drag on the side walls of the robot body [12]. Other designs include a screw mechanism [13], a crab inspired robot [14], and a deformable octahedron [15].

Combining the inspiration of tip growth in plant roots with the phenomenon of granular fluidization, we have developed a burrowing device for shallow subterranean exploration in sand. We build on a soft, pneumatic, tip-extending robot described by Hawkes et al. [16] by adding a method to deliver a flow of air out of the tip of the robot. The air flow fluidizes the surrounding sand particles, allowing the robot to grow and travel through the ground. This paper will describe the design of the device, simple models of its behavior, fabrication of a prototype, results of experimental testing, and will conclude with a brief discussion and summary.

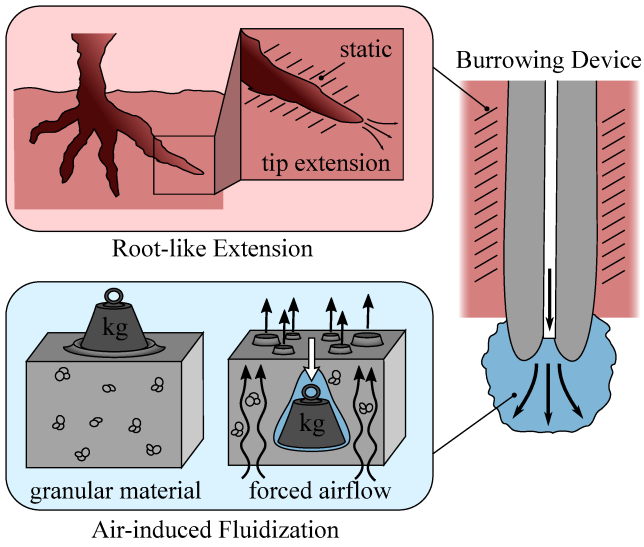

Fig. 1. The burrowing device combines principles from roots and granular medium air-fluidization for reducing resistance during subterranean motion. In roots, the tip grows while the rest of the root remains stationary, eliminating friction along the sides. In granular medium air-fluidization, air is pumped into the medium, resulting in a medium that behaves like a fluid.

II. DESIGN

A. Principles

The burrowing robot incorporates two physical principles to improve its ability to move below ground (Fig. 1). The first principle is derived from the roots of plants which grow from their tips; extending from the tip, rather than moving the whole body forward, eliminates the friction along the sides of the body. The second principle is that a granular medium

[1]Department of Mechanical Engineering, University of California, Santa Barbara, CA 93106, USA
[2]School of Physics, Georgia Institute of Technology, Atlanta, GA 30332
*Corresponding author. Email: nnaclerio@ucsb.edu

can behave like a fluid when air is passed through it [17]–[19]. This can substantially decrease the force required to pass through the medium; dense objects will even sink. We refer to this principle as air-fluidization throughout the paper.

B. Implementation

Our design incorporates these two principles in an inflated soft burrowing device (Fig. 2). The main body of the burrowing device is a pressurized thin-walled tube constructed from an inelastic membrane. The main body tubing is inverted back inside itself, such that when pressurized, the tubing everts and new material passes out of the tip. In this manner, we are able to achieve root-like tip-extension without the complexity involved in real root growth [7]. This design is similar to our previous work [16]. However, in order to aid in burrowing, we incorporate the principle of local granular air-fluidization by releasing pressurized air out of the tip of the device. The air passes through the core of the body in the fluidization tube. This tube is split lengthwise and attached to opposite sides of the main body. Therefore, as the main body everts, the fluidization tube splits and becomes part of the side of the body.

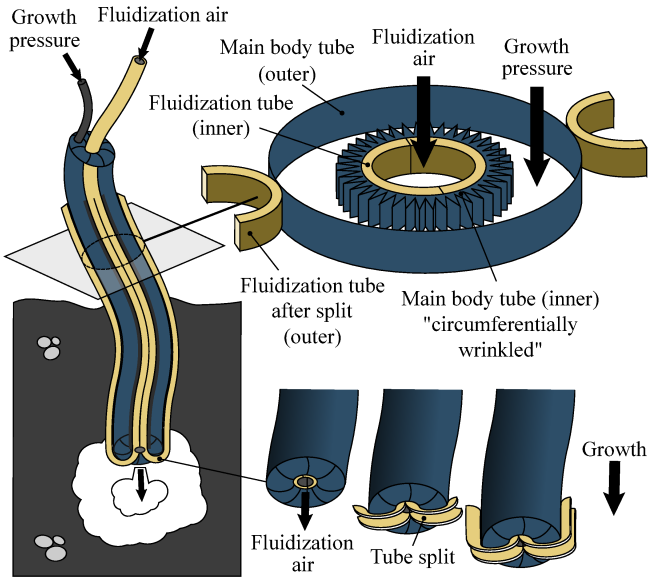

Fig. 2. Schematic drawing of the tip-extending burrowing device. The main body tube extends at its tip due to the growth pressure everting wrinkled material that passes through the core of the main body. Air flows through the fluidization tube and out of the tip of the robot. The fluidization tube runs down the core of the main body, splits at the tip, and wraps around the two sides.

III. MODELING

A. Model of Tip-extension Forces

The goal of this section is to model how different parameters affect growing forces to improve tip-extending burrowing devices. In the ideal case, the balanced forces at the tip of the robot would be:

$$F_{driving} = F_{external} \tag{1}$$

where $F_{driving}$ is equivalent to the internal pressure, P, times the cross-sectional area, A, and $F_{external}$ is the net growing force pushing against the medium. However, in reality, not all of the driving force, PA, is transferred to the medium. The actual force transferred to the medium, $F_{external}$, can be approximated by the addition of a proportional term, k, and an offset term, F_{offset}, leading to

$$F_{driving}k - F_{offset} = F_{external}. \tag{2}$$

The proportional term arises largely from axial tension in the body of the device that partially counters the driving force. For the offset force, Blumenschein et al. [20] showed that

$$F_{offset} = [YA + F_v] - [F_l + \Sigma_i F_{Ci}] \tag{3}$$

where Y is the yield pressure under which no growth occurs, and F_v, F_l, and F_{Ci} are the velocity, length, and curvature dependent force terms respectively. For our case of straight, slow, shallow growth these terms are negligible and this reduces to

$$F_{offset} = YA. \tag{4}$$

Blumenschein et al. also found that YA is constant for a given tube material, and independent of tube diameter. Thus, F_{offset} is constant among identically constructed devices of different diameters. Therefore, once k and F_{offset} are determined for a given burrowing device, the external force, $F_{external}$, can be predicted from the internal pressure, P:

$$F_{external} = PAk - F_{offset}. \tag{5}$$

For the device to burrow, the external force it exerts must be greater than the counteracting force of the medium into which it is burrowing (F_{medium}). In other words:

$$F_{medium} < F_{external} = PAk - F_{offset}. \tag{6}$$

B. Radius for Maximum Tip-extension Force

It is also possible to predict the radius of body that would enable the largest external pressure applied to the granular medium before bursting, due to hoop stress in the body. Using the equation for hoop stress in a thin-walled pressure vessel, the internal pressure can be written as

$$P = \sigma_\theta t / r \tag{7}$$

where σ_θ is hoop stress, t is wall thickness, and r is radius. Substituting in the yield stress, σ_y, and inserting back into Eqn. 5 along with $F_{external} = P_{external}A$ and $A = \pi r^2$ we have

$$\frac{\sigma_y t k}{r} - \frac{F_{offset}}{\pi r^2} = P_{external}. \tag{8}$$

We again assume that F_{offset} is independent of diameter. Taking the derivative with respect to r, setting it to zero, and solving for r, we find that the maximum external pressure is at the following radius

$$r = \frac{2F_{offset}}{\pi \sigma_y t k} \tag{9}$$

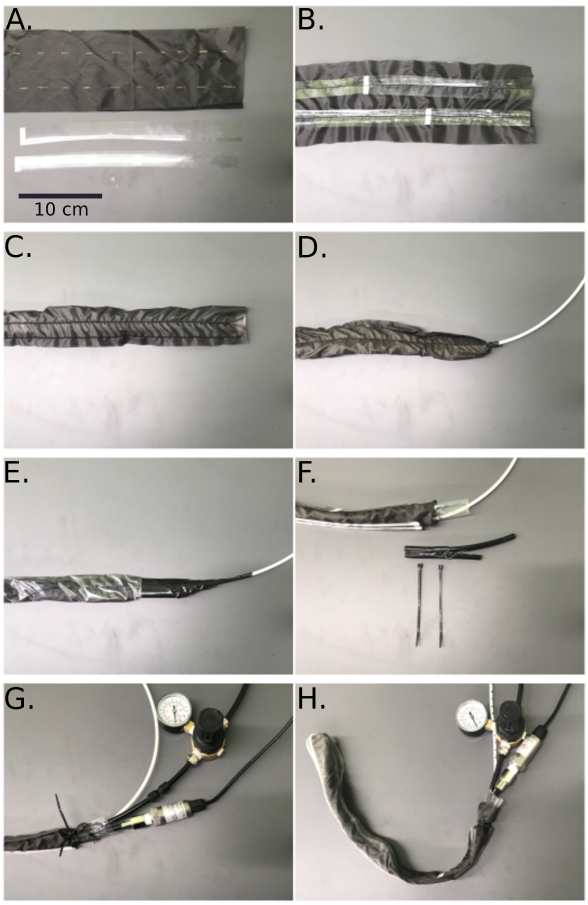

Fig. 3. Sequence of photographs showing the fabrication of the burrowing device. As described in Sec. IV, the black tube is the outer tube, the clear strips and white tube make up the fluidization tube, and the clear plastic tube is the inner-tube. All figures are to the same scale. See Sec. IV for fabrication details.

IV. FABRICATION

The main components of our prototype robotic burrowing device are: a 2.7 cm diameter outer-tube made of 0.05 mm thick rip-stop nylon fabric sewn together with nylon thread, a 2.7 cm diameter inner-tube made of 0.05 mm thick low density polyethylene (LDPE), a fluidization tube made of a flexible 8 mm outer-diameter tube and 0.125 mm thick acetate strips with hot glue. The outer-tube determines the device's shape and robustness, the inner tube provides a good air seal, and the fluidization tube provides a flow of air out of the tip of the device.

The manufacturing steps are as follows, and correspond to the sub-figures in Fig. 3: (A) Cut a strip of nylon fabric to device length and slightly wider than tube circumference (about 10 cm). (B) Sew two strips of acetate along the length of the nylon fabric, spaced apart so that they will lay flat on each other when the nylon fabric is folded in half lengthwise. Hot glue two beads of glue along the length of one of the strips, spaced evenly apart. As the acetate strips lay against each other, the gap created between them by the glue is the fluidization tube shown in Fig. 2. (C) Fold the fabric in half lengthwise and sew along the edge, creating a tube. (D) Attach the fluidization tube to the inside of the fabric tube, between the acetate strips such that air will flow into the fabric tube, and into the fluidization tube between the acetate strips. (E) Slide the inner tube over the completed outer tube and tape to the fluidization tube. (F) Invert the inner tube, and then the outer tube over it. Prepare three short air tubes; one for the growth pressure, a second for a pressure sensor, and a third for the fluidization tube to pass through. (G) Seal the inner and outer tubes around the air tubes, allowing the fluidization tube to pass through one of them. (H) The completed device will now grow when pressurized by the growth pressure, pulling the fluidization tube along with it. Air can flow out of the tip through the fluidization tube. Growth is reversed by retracting the fluidization tube.

V. RESULTS

A. Verification of Model

We ran a set of tests to verify our model that predicts the force that the tip-extending burrowing device applies to the medium, as described in Eqn. 5. This prediction of force is based on the internal pressure as well as the material and geometry of the body. First, we measured the external force applied by a tip-extending device made of 0.05 mm LDPE, with a diameter of 5.1 cm. This data was used to determine that the values of k and F_{offset} were 4.0 and 0.38 N respectively, for this thickness of LDPE. These constants were fed into the model, which was then used to predict the behavior of two other sized devices of identical construction and diameters of 2.4 cm and 1.6 cm. The comparison between the predicted and measured external force for a range of pressures is shown in Fig. 4.

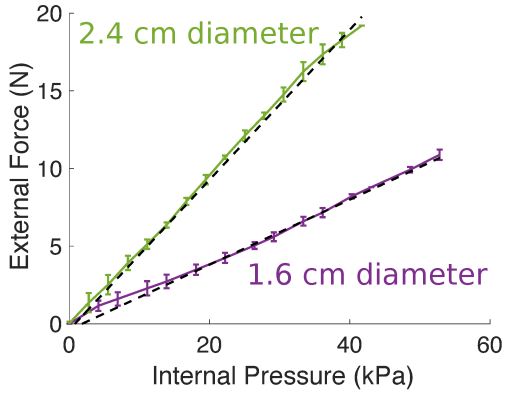

Fig. 4. Comparison between experimental data (solid, colored lines) and model predictions (dashed black lines) based on Eqn. 5 for two different sized main body tube diameters.

B. Characterization of Effects of Tip-extension and Tip-flow

We conducted a series of tests to help characterize the behavior of the burrowing device in common store-bought play sand with most grain sizes ranging from 1 mm to 0.1 mm in width.

1) Effect of Tip-Flow on Burrowing Force: Our first set of tests were designed to isolate and characterize the effect of tip airflow on intrusion force, for which we performed a controlled intrusion experiment using a robotic arm. Unlike the presented robotic burrowing device design, this test intrusion apparatus employed a passive rigid intruder. We 3D-printed an ABS plastic cylindrical intruder (outer diameter of 2.7 cm) and inserted a pneumatic tube (inner diameter of 5 mm) down through the central axis of the intruder and out through the tip to provide fluidization air. We used a regulated air supply and measured the flow of the air with an Omega FMA 1845 mass flowmeter. Before each experiment we measured the pressure of the air from open end of the pneumatic tube with a Honeywell 030PGAA5 pressure sensor using an Arduino Uno.

To execute a position-controlled intrusion maneuver, the intruder was mounted on to the end-effector of a 6-axis Denso robot arm. An ATI Mini 40 force/torque sensor was mounted between the arm and intruder, facilitating intrusion force measurement. For each experiment, the robot was commanded to slowly intrude (0.5 cm/s) vertically into a fluidized bed of play sand. Intrusions were performed with fluidization air at volumetric flow rates of 0, 5, 10, and 15 L/min, and five trials were collected per flow rate. Prior to each experiment, the state of the play sand was reset via bed-fluidization, a process where blowers force air through the porous bottom of the fluidized bed, causing the sand to bubble. After bubbling ceases, the sand is in a loosely packed state with a relatively flat surface. To more-closely mirror the closer material packing of a natural setting, the bed was subsequently shaken with a vibration motor and then manually compacted with a rigid flat plate.

We report the results of this test using force vs. depth curves, as shown in Fig. 5. There is a significant decrease in the force required to move through the medium as the tip-flow increases. At the maximum depth measured, the force difference between the no-flow case and the peak-flow case was approximately a factor of 50. Note, because forced air flow also has the property of eroding some material away before contact, depth is measured from the point of first contact with non-airborne sand.

2) Visualization of Effects of Tip-flow: To further understand the effects of the flow of air out of the tip of the device, we performed similar intrusion experiments (as above) but with a transparent wall. For this purpose, we 3D-printed another intruder out of ABS plastic, but with a flattened side to slide directly adjacent to a side wall. We commanded the intruder along a transparent acrylic side wall of the fluidized bed and recorded the motion with AOS high speed camera at 250 fps. Screen captures from these videos are shown in Fig. 6, at three different depths and four different tip-flows (a video from this test can be seen in the accompanying video). With 5 L/min of flow, a small air channel emerges that shows a small aerated region beneath the intruder. Higher tip-flow creates a visibly larger fluidized area for the 10 and 16 L/min cases. For these experiments the wall effects may alter the air flow patterns to some degree, however, the measured forces

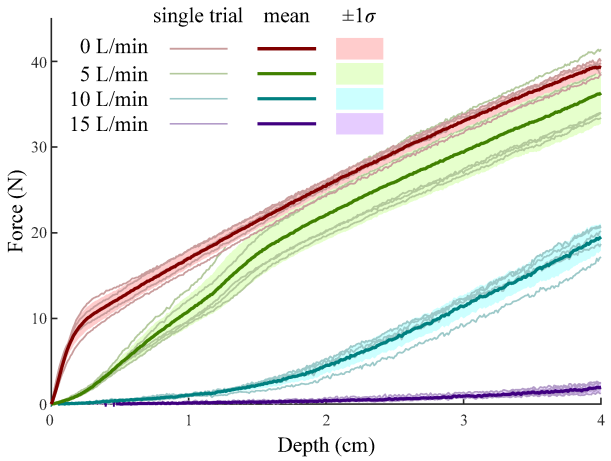

Fig. 5. Data showing that increased tip air-flow rates change the relationship between the force and depth, while significantly decreasing the force at all depths. These tests were conducted with a passive intruder pushed into the medium.

during this experiment are in accord with those reported in Figure 5 which were far from the boundary.

3) Effect of Tip-extension on Burrowing Force: To characterize the effect of tip-extension on the force versus depth relationship for a burrowing device, we extended a burrowing device into play sand and compared it to a passive intruder, neither with tip air flow. The burrowing device we used is described in Sec. IV. The sand was placed in a 25 cm cube container with a sand depth of 20 cm, and was briefly fluidized between each trial to help create a repeatable packing density. For data with the intruder, we used a Mark-10 M3-100 force gauge in series with the intruder to measure the force required to move into the sand as a function of depth for five trials. The intruder for this test was identical to the one used in V-B.1 and was the same diameter as the tip-extending burrowing device. For data with the tip-extending burrowing device, we measured the internal pressure with a Dwyer 628 0-100 psi pressure transmitter using an Arduino Uno, which was then used to calculate the force applied to the sand using Eqn. 5. Six trials were performed measuring internal pressure as a function of burrowing depth. The results of these tests are shown in Fig. 7. The addition of tip-extension creates a decrease in the required force at any given depth. Note that the tip-extending device could not intrude as deep as the passive intruder because the growth pressure required to continue would exceed the device's bursting pressure.

4) Tip-flow in Combination with Tip-extension: Finally, we tested the tip-extending burrowing device with tip-flow. Based on the results shown in Fig. 5, we chose the highest level of tip-flow that was achievable in our setup (24 L/min). Measurements of pressure as a function of depth were recorded for six trials, and converted to force vs. depth by Eqn. 5. The results of the tests are shown in Fig. 7. The slope of the force versus depth curve is decreased by over an order of magnitude when compared to that of a passive intruder with no tip-flow. A separate demonstration of the

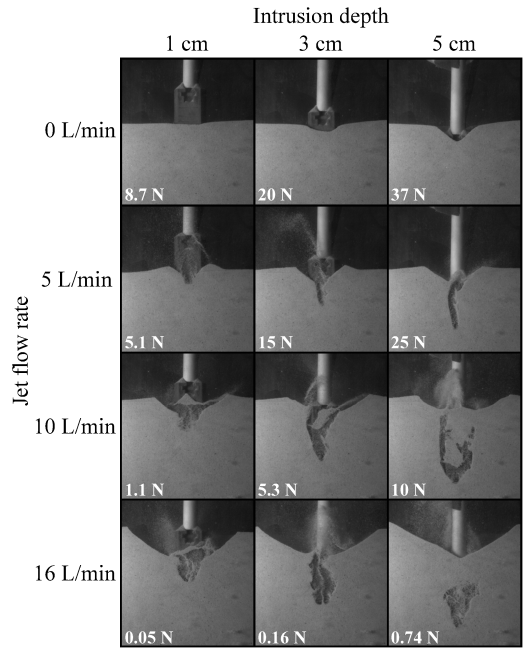

Fig. 6. Images showing the effect of flow on the medium during intrusion without tip extension. Four levels of flow are used, ranging from 0 to 16 L/min, and for each flow level, three images are taken at depths of 1 cm, 3 cm, and 5 cm. Vertical forces at each frame capture are reported in each image. Note: depths are measured relative to the first point of contact between intruder and non-airborne sand.

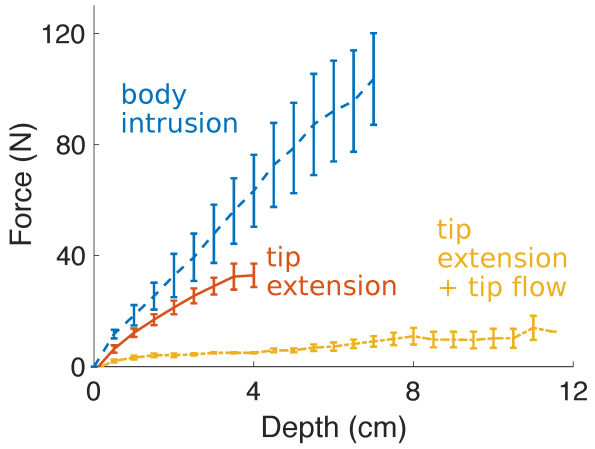

Fig. 7. Data showing the force applied to the medium as a function of depth for a passive intruder pushed into the medium with no tip-flow (blue dashed line), a tip-extending burrowing device with no tip-flow (orange solid line), and a tip-extending burrowing device with tip flow (24 L/min)

device burrowing can be seen in the accompanying video.

VI. Discussion

The results presented in Sec. V show some of the interesting behaviors of the presented mode of subterranean locomotion, which combines tip-extension with granular air-fluidization. In Fig. 5, the effect of tip-flow during body intrusion is clear in both the shapes of the curves as well as the magnitude of the forces. In the no-flow case, we observe the expected "knee" in the curve, which results from a cone of particles accumulating at the tip and reducing the resistance to further motion [21]. As tip-flow is added to the system in the range of 5 L/min, this knee disappears. Higher flow rates result in another effect, which can be visualized in Fig. 6: the tip flow completely removes sand from in front of the intruder, such that the force drops to zero for low depths. Interestingly, through 10 L/min, the slopes of the depth versus force curves remain the same.

When tip-extension is considered, shown in Fig. 7, we observe a flattening out of the force versus depth curve as depth increases. This could be due to the elimination of drag on the sides of the body, which contributes to the increasing force on the simple intruder. The tip-extension device without tip flow, however, could not pass beyond 4 cm. Referring to Eqn. 6, the robot will stop growing once the resisting force of the medium (F_{medium}, which increases with depth) exceeds the force that the robot can apply to the environment at its tip ($F_{external}$). The achievable depth can be increased with a higher driving pressure, a stronger body material, or a reduction of the resisting force of the medium, for instance through fluidization. With tip-flow and the resulting fluidization, we see an extremely flattened force versus depth curve, allowing the device to reach beyond 10 cm with well below 20 N of force.

VII. Conclusion

We have presented a prototype of a burrowing device that uses the principles of both tip-extension from plant root growth and granular medium air-fluidization. Our experiments confirm our basic model of growth forces, and show that the force to burrow into sand is reduced noticeably by tip-extension, and significantly by air-fluidization. Future work could investigate the performance of the device in other mediums including soil and damp sand, as well as its performance with other fluidization fluids such as water.

With further development, this single degree of freedom (DOF) design could be extended into a multi-DOF robot based on the concepts shown in existing soft, steerable, growing robots [16,22] to navigate in shallow, subterranean, granular environments. This technology could be used for a wide range of applications including search and rescue in mudslides, the non-invasive installation of underground irrigation or communication lines, and as a root-like foundation structure.

Acknowledgment

Thank you to Zhiwei Zhang and Aaron Nguyen at UCSB for their help developing and testing the robotic burrowing device.

References

[1] R. D. Maladen, Y. Ding, P. B. Umbanhowar, A. Kamor, and D. I. Goldman, "Mechanical models of sandfish locomotion reveal principles of high performance subsurface sand-swimming," *Journal of The Royal Society Interface*, vol. 8, no. 62, pp. 1332–1345, 2011.

[2] E. Shuter and W. E. Teasdale, *Application of drilling, coring, and sampling techniques to test holes and wells*. Department of the Interior, US Geological Survey, 1989, vol. 2.

[3] G. Girmscheid and C. Schexnayder, "Tunnel boring machines," *Practice periodical on structural design and construction*, vol. 8, no. 3, pp. 150–163, 2003.

[4] G. P. Tsinker, "Performance of jetted anchor piles with widening," *Journal of Geotechnical and Geoenvironmental Engineering*, vol. 103, no. 3, 1977.

[5] A. Hosoi and D. I. Goldman, "Beneath our feet: strategies for locomotion in granular media," *Annual Review of Fluid Mechanics*, vol. 47, 2015.

[6] R. D. Maladen, P. B. Umbanhowar, Y. Ding, A. Masse, and D. I. Goldman, "Granular lift forces predict vertical motion of a sand-swimming robot," in *Robotics and Automation (ICRA), 2011 IEEE International Conference on*. IEEE, 2011, pp. 1398–1403.

[7] A. Dexter, "Mechanics of root growth," *Plant and soil*, vol. 98, no. 3, pp. 303–312, 1987.

[8] A. Koller-Hodac, D. P. Germann, A. Gilgen, K. Dietrich, M. Hadorn, W. Schatz, and P. E. Hotz, "Actuated bivalve robot study of the burrowing locomotion in sediment," in *Robotics and Automation (ICRA), 2010 IEEE International Conference on*. IEEE, 2010, pp. 1209–1214.

[9] A. G. Winter, R. L. Deits, D. S. Dorsch, A. E. Hosoi, and A. H. Slocum, "Teaching roboclam to dig: The design, testing, and genetic algorithm optimization of a biomimetic robot," in *Intelligent Robots and Systems (IROS), 2010 IEEE/RSJ International Conference on*. IEEE, 2010, pp. 4231–4235.

[10] A. Winter, R. Deits, D. Dorsch, A. Slocum, A. Hosoi *et al.*, "Razor clam to roboclam: burrowing drag reduction mechanisms and their robotic adaptation," *Bioinspiration & biomimetics*, vol. 9, no. 3, p. 036009, 2014.

[11] A. Sadeghi, A. Tonazzini, L. Popova, and B. Mazzolai, "Robotic mechanism for soil penetration inspired by plant root," in *Robotics and Automation (ICRA), 2013 IEEE International Conference on*. IEEE, 2013, pp. 3457–3462.

[12] A. Sadeghi, A. Mondini, and B. Mazzolai, "Toward self-growing soft robots inspired by plant roots and based on additive manufacturing technologies," *Soft robotics*, vol. 4, no. 3, pp. 211–223, 2017.

[13] K. Nagaoka, T. Kubota, M. Otsuki, and S. Tanaka, "Experimental study on autonomous burrowing screw robot for subsurface exploration on the moon," in *Intelligent Robots and Systems, 2008. IROS 2008. IEEE/RSJ International Conference on*. IEEE, 2008, pp. 4104–4109.

[14] R. A. Russell, "Crabot: A biomimetic burrowing robot designed for underground chemical source location," *Advanced Robotics*, vol. 25, no. 1-2, pp. 119–134, 2011.

[15] J. C. Zagal, C. Armstrong, and S. Li, "Deformable octahedron burrowing robot." in *ALIFE*, 2012.

[16] E. W. Hawkes, L. H. Blumenschein, J. D. Greer, and A. M. Okamura, "A soft robot that navigates its environment through growth," *Science Robotics*, vol. 2, no. 8, p. eaan3028, 2017.

[17] S. Sundaresan, "Instabilities in fluidized beds," *Annual review of fluid mechanics*, vol. 35, no. 1, pp. 63–88, 2003.

[18] D. I. Goldman and H. L. Swinney, "Signatures of glass formation in a fluidized bed of hard spheres," *Physical review letters*, vol. 96, no. 14, p. 145702, 2006.

[19] B. D. Texier, A. Ibarra, and F. Melo, "Low-resistive vibratory penetration in granular media," *PloS one*, vol. 12, no. 4, p. e0175412, 2017.

[20] L. H. Blumenschein, A. M. Okamura, and E. W. Hawkes, "Modeling of bioinspired apical extension in a soft robot," in *Conference on Biomimetic and Biohybrid Systems*. Springer, 2017, pp. 522–531.

[21] J. Aguilar and D. I. Goldman, "Robophysical study of jumping dynamics on granular media," *Nature Physics*, vol. 12, no. 3, p. 278, 2016.

[22] J. D. Greer, T. K. Morimoto, A. M. Okamura, and E. W. Hawkes, "Series pneumatic artificial muscles (spams) and application to a soft continuum robot," in *Robotics and Automation (ICRA), 2017 IEEE International Conference on*. IEEE, 2017, pp. 5503–5510.